Thermal neutron capture cross sections of the palladium isotopes

M. Krtička,[1,2] R. B. Firestone,[3] D. P. McNabb,[4] B. Sleaford,[4] U. Agvaanluvsan,[4] T. Belgya,[5] and Z. S. Revay[5]
[1]*Charles University in Prague, Faculty of Mathematics and Physics, V Holešovičkách 2, CZ-180 00 Prague 8, Czech Republic*
[2]*North Carolina State University, Raleigh, NC 27695, USA*
[3]*Lawrence Berkeley National Laboratory, Berkeley, CA 94720, USA*
[4]*Lawrence Livermore National Laboratory, L-414, 7000 East Avenue, Livermore, CA 94551, USA*
[5]*Institute of Isotope and Surface Chemistry, H-1525, Budapest, Hungary*
(Received 12 October 2007; published 30 May 2008)

Precise thermal neutron capture γ-ray cross sections σ_γ were measured for all elements with $Z = 1$–83, 90, and 92, except for He and Pm, at the Budapest Reactor. These data were evaluated with additional information from the literature to generate the Evaluated Gamma-ray Activation File (EGAF). Isotopic radiative neutron cross sections can be deduced from the total transition cross section feeding the ground state, $\sigma_0 = \Sigma\sigma_\gamma(\mathrm{GS})$ if the decay scheme is complete. The EGAF file contains partial γ-ray cross sections for all stable palladium isotopes. None of these decay schemes are complete, although in each case transitions de-exciting low-lying levels are known. We have performed Monte Carlo simulations of the palladium thermal neutron capture decay schemes using the computer code DICEBOX. The simulated populations of low low-lying levels are normalized to the measured σ_γ values from EGAF and the total radiative neutron cross section σ_0 is obtained. The σ_0 values derived for the palladium isotopes agree well with previous measurements and were in several cases more precise. Complementary use of γ-ray cross-section data and Monte Carlo calculations has proven effective in determining both the palladium total radiative cross sections and new nuclear structure information.

DOI: 10.1103/PhysRevC.77.054615 PACS number(s): 23.20.Lv, 24.10.Lx, 24.60.Dr, 25.40.Lw

I. INTRODUCTION

Total radiative thermal neutron capture cross sections are typically determined by measuring the neutron transmission rate through a target or by determining the activation rate of a radioactive product. Both methods require either knowledge of the neutron flux or use of a comparator material of well-known cross section. Transmission rates may be subject to significant corrections for neutron scattering and uncertainties in the target geometry. Activation measurements are typically more accurate but they also require normalization to a comparator, typically gold, and they rely on the accuracy of the decay scheme. Nearly all thermal neutron capture cross sections have been measured using moderated reactor neutrons where the flux of epithermal, fast, and high-energy neutrons is considerable and must be accounted for.

In this article we report a new method for the determination of total radiative thermal neutron capture cross sections using prompt neutron capture γ rays measured with guided thermal neutron beams at the Budapest Reactor. The neutron beams contain no epithermal, fast, or high-energy components. Prompt γ-ray neutron capture cross sections were measured far from the reactor core where background radiation is low and both the primary transitions de-exciting the capture state and secondary transitions feeding the ground state can be observed. For low-Z isotopes complete neutron capture decay schemes were measured, leading to redundant determination of the total cross section from both the primary and secondary transitions. For high-Z isotopes measurement of primary and secondary γ-ray cross sections were generally incomplete. To determine the total radiative neutron capture cross sections for high-Z isotopes, the measured decay scheme must be corrected for the contribution from unobserved continuum γ rays.

We measured thermal neutron capture γ-ray cross sections on a natural palladium target. Transition cross sections were observed for all stable palladium isotopes. Extensive decay schemes were observed for ^{106,109}Pd and only a few transitions were observed for ^{103,105,107,111}Pd. We then performed statistical model calculations with the Monte Carlo computer code DICEBOX [1] to generate simulated neutron capture decay schemes, constrained by known nuclear structure properties, for the palladium isotopes. The simulated intensities of transitions between low-lying levels were normalized to the measured transition cross sections to determine the continuum cross section contribution feeding the ground state, which, added to the measured ground-state cross sections, gives the total radiative neutron capture cross section. The sensitivity of the statistical calculations to model parameters was tested, and the uncertainty in the contribution of the calculated continuum could be estimated. Total radiative neutron capture cross sections for all stable palladium isotopes were determined with an accuracy consistent to or better than previous methods.

II. EXPERIMENT

Neutron-capture γ-ray cross sections for elemental targets with $Z = 1$–83, 90, 92, except for He and Pm, have been measured at the 10-MW Budapest Reactor with a guided thermal neutron beam [2]. These data were published in the *Handbook of Prompt Gamma Activation Analysis* [3]. The target station is located ≈30 m from the reactor where both primary and secondary γ rays can be measured in low background conditions. Neutrons enter the evacuated target holder and continue to the beam stop at the rear wall of the guide hall. The thermal-equivalent neutron flux was

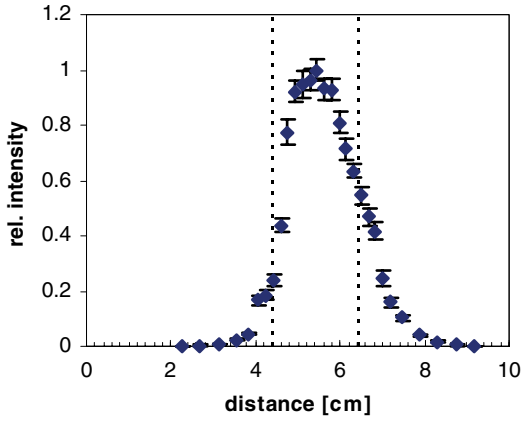

FIG. 1. Neutron flux profile as a function of distance from the base of the target holder in the guided thermal neutron beam at the Budapest Reactor.

2×10^6 n cm^2 s^{-1}. A spatial profile of the neutron beam at the target position is shown in Fig. 1.

Prompt γ rays from the target were measured with an n-type high-purity, 25% efficient, germanium (HPGe) detector with closed-end coaxial geometry located 23.5 cm from the target. The detector is Compton suppressed by a bismuth germanate (BGO) scintillator guard detector annulus surrounded by 10-cm-thick lead shielding. Counting efficiency was calibrated from 50 keV to 10 MeV with radioactive sources and (n, γ) reaction γ rays to a precision of better than 1% from 500 keV to 6 MeV and better than 3% at all energies [4]. The γ-ray spectra were analyzed using the Hypermet PC program [4,5].

Total radiative thermal neutron cross sections were determined using either stoichiometric compounds or accurately prepared mixtures containing the standard elements H, N, or Cl whose γ-ray cross sections are precisely known [6]. The γ-ray cross sections for isotopes of interest were then accurately determined from their intensity ratios to the standard γ-ray transition intensities of the comparators. These measurements are independent of target composition or neutron flux. The neutron beam used in these measurements is a pure thermal beam so the measured γ-ray cross sections do not need to be corrected for epithermal contributions.

In this experiment the most intense palladium γ rays were calibrated with respect to chlorine with a target consisting of 1.6 g of $PdCl_2$ with a thickness of 0.4 g/cm^2. A 0.15-g natural palladium powder target, suspended in a teflon bag to reduce background from the target holder, was irradiated for ≈8 h to obtain a higher statistics spectrum. Weak transition cross sections were calibrated by their relative intensities with respect to the more intense palladium γ rays. A total of 202γ rays were assigned to the six palladium isotopes ^{103}Pd, ^{105}Pd, ^{106}Pd, ^{107}Pd, ^{109}Pd, and ^{111}Pd on the basis of energy and intensity by comparison with data from the ENSDF [7] file. The γ-ray cross-section data were sufficient to determine level de-excitation cross sections for 55 ^{106}Pd levels, 31 ^{109}Pd levels, and at least 2 levels from each of the other palladium isotopes. These results are summarized in Table I.

III. STATISTICAL MODEL SIMULATIONS

Theoretical feeding of low-lying levels by thermal neutron radiative capture was calculated using the computer code DICEBOX [1]. The algorithm of this Monte Carlo code is based on the generalization of the extreme statistical model, embodying Bohr's idea of a compound nucleus [8]. Below a certain *critical* energy, $E_{\rm cut}$, the level scheme, i.e., energies, spins, and parities of all levels, as well as all de-exciting transitions, is taken from experiment. Above $E_{\rm cut}$, a set of levels is generated as a random discretization of an *a priori* known level-density formula $\rho(E, J^\pi)$. Decay properties of an initial level i above $E_{\rm cut}$ are completely characterized by a full set of partial radiation widths to all final levels f below the level i. A partial radiative width, $\Gamma_{i\gamma f}$, that characterizes the probability of γ-ray decay with an energy $E_\gamma = E_i - E_f$ is assumed to be a random choice from the Porter-Thomas distribution [9] with a mean value

$$\langle \Gamma_{i\gamma f} \rangle = \frac{f^{(XL)}(E_\gamma, \xi) \times E_\gamma^3}{\rho\left(E_i, J_i^\pi\right)}. \quad (1)$$

Here, $\rho(E_i, J_i^\pi)$ is the level density near the initial level i and $f^{(XL)}(E_\gamma, \xi)$ is the photon strength function (PSF) for a transition of given type X and multipolarity L. The argument ξ of the PSF represents possible dependence on quantities other than γ-ray energy. In the extreme statistical model it is assumed that the $\Gamma_{i\gamma f}$ are uncorrelated. Selection rules for different types of transitions are fully accounted for in the generation of $\Gamma_{i\gamma f}$.

The random generation of a system of all $\Gamma_{i\gamma f}$, which fully describes the decay properties of the nuclear levels, is called a *nuclear realization*. Due to fluctuations involved there exists an almost infinite number of nuclear realizations that differ in decay properties even for a single choice of $f^{(XL)}$ and level density. Consequently, all simulated quantities are subject to statistical fluctuations arising from different nuclear realizations. Determination of these fluctuations with the DICEBOX code allows us to estimate the uncertainty coming from statistical nature of decay process. Typically a calculation consisted of 50 nuclear realizations, each with 30,000 capture state decays, generated by the Monte Carlo method. DICEBOX stores the simulated capture state de-excitation data that are used to calculate the intensity, per neutron capture, populating levels below $E_{\rm cut}$ and the total radiation width $\Gamma_\gamma^{\rm tot}$. The simulated level populations per neutron capture are renormalized to absolute cross sections by comparison with the experimental γ-ray cross sections depopulating these levels. The total radiative neutron capture cross section σ_0 is then defined as

$$\sigma_0 = \Sigma\sigma_\gamma^{\rm exp}({\rm GS}) + \Sigma\sigma_\gamma^{\rm sim}({\rm GS}), \quad (2)$$

where $\Sigma\sigma_\gamma^{\rm exp}$(GS) is the sum of γ-ray cross sections populating the ground state from experimentally observed levels and $\Sigma\sigma_\gamma^{\rm sim}$(GS) is the simulated sum of γ-ray cross sections populating the ground state from all other levels. If the cross sections of primary transitions to levels below $E_{\rm cut}$ were measured, as in ^{106}Pd and ^{109}Pd, they were used in all nuclear realizations. Otherwise the intensities of primary transitions

TABLE I. Palladium thermal neutron capture γ-ray energies and cross sections measured in this work. Values in brackets are calculated from adopted branching intensities in the Evaluated Nuclear Structure Data File (ENSDF) [7].

Level (keV)	J^π	E_γ (keV)	σ_γ barns	Level (keV)	J^π	E_γ (keV)	σ_γ barns	Level (keV)	J^π	E_γ (keV)	σ_γ barns
^{103}Pd				2083.9	3^-	522.0(3)	0.010(4)	2713.6	$2^+,3^+$	1155.96(10)	0.061(7)
0	$5/2^+$					956.23(9)	0.087(9)			1484.5(3)	0.039(9)
118.7	$3/2^+$	118.53(18)	0.42(11)			1572.57(9)	0.99(13)			[2202.07(15)]	[0.018]
504.2	$(3/2)^+$	[237.3(2)]	[0.055]			[2084.0(4)]	[0.0035]	2741.0	$(1,2^+)$	[2229.5(10)]	[0.34]
		385.4(4)	0.40(14)	2242.5	2^+	680.17(5)	0.173(10)			2740.57(24)	0.66(9)
		[504.2(1)]	[0.14]			[684.80(20)]	[0.073]	2748.2	$2,3^-$	2235.92(15)	0.157(13)
^{105}Pd						1108.67(16)	0.067(10)	2757.0	5^+	[178.2(5)]	[0.00004]
0	$5/2^+$					1114.37(8)	0.170(13)			[391.039(30)]	[0.0008]
280.5	$3/2^+$	280.65(6)	0.142(13)			[1730.35(23)]	[0.030]			[406.17(3)]	[0.010]
306.2	$7/2^+$	306.26(18)	0.039(8)			[2242.46(12)]	[0.027]			451.29(25)	0.021(8)
344.5	$1/2^+$	[63.98(3)]	[0.036]	2282.9	4^+	1053.69(6)	0.260(13)			[474.060(30)]	[0.0007]
		344.11(11)	0.061(11)			[1771.1(3)]	[0.011]			[680.420(10)]	[0.0012]
442.4	$(7/2)^+$	442.11(21)	0.047(16)	2305.6	4^-	221.78(4)	0.118(6)			824.59(15)	0.027(6)
560.8	$3/2^+$	[216.17(15)]	[0.002]			228.69(8)	0.054(5)			[1199.39(10)]	[0.0084]
		560.67(20)	0.048(10)			748.33(3)	0.359(10)			[1527.65(19)]	[0.012]
644.5	$7/2^-$	[155.39(6)]	[0.003]			[1077.2(5)]	[0.0009]	2774.9	(4^+)	533.66(18)	0.021(6)
		[202.13(16)]	[0.00007]			[1178.07(21)]	[0.0034]			[1218.26(14)]	[0.033]
		[325.26(7)]	[0.0009]			[1794.01(27)]	[0.0006]			[1546.64(16)]	[0.012]
		644.76(13)	0.059(6)	2350.8	4^+	[418.71(28)]	[0.0060]			2263.2(5)	0.036(18)
7094.1	$1/2^+$	6812.5(4)	0.133(11)			793.35(7)	0.114(8)	2783.8	2^+	[1554.50(15)]	[0.0046]
^{106}Pd						[1121.60(18)]	[0.0092]			[1655.66(17)]	[0.0092]
0	0^+					1222.96(13)	0.114(10)			2271.82(19)	0.125(13)
511.9	2^+	511.847(13)	17.9(2)			1839.2(5)	0.037(10)	2821.0	2^+	[1258.80(20)]	[0.011]
1128.0	2^+	616.219(15)	2.81(4)	2366.0	5^+	[433.9(4)]	[0.0024]			[1687.40(30)]	[0.011]
		1127.99(3)	1.45(3)			808.36(7)	0.107(10)			[1693.20(30)]	[0.012]
1133.8	0^+	621.97(5)	0.56(3)			[1136.85(19)]	[0.0061]			2308.97(20)	0.082(10)
		[1133.7(7)]	[0.0003(E0)[a]]	2397.5	$(5)^-$	1168.13(5)	0.264(10)			[2821.10(30)]	[0.023]
1229.2	4^+	717.349(14)	3.48(4)	2401.4	$2^-,3^-$	1272.85(6)	0.188(13)	2828.3	0^+	[1266.00(20)]	[0.0091]
1557.6	3^+	328.49(13)	0.043(7)			1889.25(18)	0.112(13)			2316.9(3)	0.056(10)
		429.69(3)	0.649(13)	2439.1	2^+	[1209.80(20)]	[0.0057]	2850.4	$2^+,3^+$	1621.44(17)	0.088(11)
		1045.77(3)	1.44(3)			1305.6(4)	0.029(10)	2861.0	$(^+)$	1302.69(19)	0.055(9)
1562.2	2^+	428.46(6)[c]	0.11(2)			1926.96(14)	0.197(18)			[1631.7]	[0.028]
		[434.25(21)]	[0.002]			2439.01(23)	0.090(13)	2877.9	0^+	[1315.7(2)]	[0.0046]
		1050.30(3)	1.61(4)	2472.7	$1^+,2^+$	471.29(15)	0.029(6)			2365.1(7)	0.031(13)
		1562.07(10)	0.157(13)			765.8(6)	0.020(10)	2886.5	$(^-)$	2374.0(3)	0.094(13)
1706.4	0^+	578.89(11)	0.053(6)			[1960.17(20)]	[0.024]	2897.8	$(1^-,4^-)$	1668.40(23)	0.044(8)
		1194.54(6)	0.145(8)	2484.7	(1^-)	[1973.5(10)]	[0.046]	2902.5	2^+	1773.8(4)	0.031(13)
1909.4	2^+	346.92(16)	0.043(8)			2484.37(15)	0.228(18)			2390.79(22)	0.094(13)
		775.72(16)	0.082(10)	2500.3	2^-	[942.6(4)]	[0.0059]			[2902.5(8)]	[0.0009]
		[781.6(5)]	[0.009]			[1372.30(30)]	[0.021]	2908.7	(1^-)	2396.57(13)	0.179(13)
		1397.52(5)	0.399(13)			1988.06(10)	0.27(8)	2917.9	2^+	1355.1(4)	0.021(9)
		1909.42(8)[c]	0.103(22)	2578.4	(4^-)	[1020.7(3)]	[0.075]			1360.6(3)	0.032(9)
1932.3	4^+	374.0(4)	0.006(5)			1349.44(9)	0.150(11)			[1784.1(3)]	[0.0025]
		703.14(6)	0.152(10)	2591.2	$(2,3)^+$	659.53(8)	0.063(6)			2405.56(20)	0.085(13)
		804.34(3)	0.407(13)	2624.4	0^+	[1062.14(5)]	[0.012]			2918.0(4)	0.040(13)
		[1419.4(8)]	[0.0011]			[1496.33(13)]	[0.0084]	2936.0	$(2^-,3^-)$	2423.69(19)	0.103(16)
2001.5	0^+	[439.19(26)]	[0.0024]			2111.9(4)	0.013(6)	2968.7	3^-	2456.3(4)	0.09(3)
		873.51(9)	0.084(8)	2626.9	$(2,3)^+$	1063.8(5)	0.026(10)	3037.3	1,2	1909.42(8)[c]	0.07(2)
		[1489.60(19)]	[0.0041]			2114.68(19)	0.048(7)			[2525.2(6)]	[0.010]
		[2002(1)]	[0.02(E0)[a]]	2705.3	$(1)^+$	[702.8(10)]	[0.0073]			3036.4(7)	0.067(13)
2076.3	6^+	848.11(4)[b]	0.103(22)			[1572.40(20)]	[0.0046]	3055.0	1^+	1498.67(10)	0.118(11)
2076.6	4^+	848.11(4)[b]	0.345(22)			1577.7(5)	0.031(13)			2543.9(6)	0.045(13)
		[949.52(25)]	[0.041]			2192.72(21)	0.121(13)			[3055.0(4)]	[0.0059]
		1565.73(14)	0.085(13)			2705.2(4)	0.031(13)	3069.9	$(2,3)^-$	2559.04(23)	0.121(13)

TABLE I. *(Continued.)*

Level (keV)	J^π	E_γ (keV)	σ_γ barns	Level (keV)	J^π	E_γ (keV)	σ_γ barns	Level (keV)	J^π	E_γ (keV)	σ_γ barns
3083.5	0	[1954.6(4)]	[0.0062]			426.17(8)	0.060(7)			674.25(13)	0.0034(6)
		2571.2(4)	0.049(13)	433.6	$3/2^+$	106.6(4)	0.011(7)			696.23(20)	0.029(7)
3161.1	2^+	[1602.2(12)]	[0.023]			108.46(18)	0.029(8)	945.0	$1/2^+$	[222.922(6)]	[0.0038]
		2649.0(3)	0.098(11)			320.29(11)	0.15(4)			[653.505(36])	[0.0050]
3221.4	0^+	[2093.3(4)]	[0.0035]			433.602(25)	0.367(11)			678.673(41)	[0.0072]
		2709.4(4)	0.036(13)	491.6	$3/2^+$	166.61(13)	0.0159(23)			831.44(7)	0.072(5)
3252.0	2^+	2740.57(24)	0.0066(9)			200.24(6)	0.073(5)	954.2	$1/2^+$	520.47(10)	0.039(5)
9561.4	$2^+, 3^+$	6490.3(5)	0.072(11)			378.22(4)	0.155(8)			628.96(20)	0.022(7)
		6625.1(5)	0.081(13)			491.70(6)	0.0174(5)			840.61(10)	0.050(5)
		6652.3(5)	0.076(13)	540.7	$5/2^+$	[213.806(4)]	[0.011]	981.8	$5/2^+$	555.40(13)	0.031(4)
		7061.0(5)	0.028(5)			215.16(8)	0.058(5)			655.14(12)	0.037(5)
		7076.9(4)	0.043(6)			249.29(5)	0.128(8)			690.17(19)	0.031(7)
		7120.7(4)	0.065(9)			[264.378(11)]	[0.0089]			[705.433(47)]	[0.0056]
		7159.9(5)	0.037(7)			[274.328(7)]	[0.0026]	1053.6	$3/2^+$	726.67(12)	0.054(7)
		7629.9(4)	0.152(13)	540.7	$5/2^+$	295.44(18)	0.010(3)			787.38(17)	0.033(6)
^{107}Pd						[540.697(10)]	[0.015]	1134.7	1/2,3/2	461.34(5)	0.087(5)
0	$5/2^+$			604.5	$5/2^-$	264.90(6)	0.084(3)			530.07(12)	0.026(4)
115.7	$1/2^+$	115.86(7)	0.052(5)			317.0(3)	0.012(4)	1232.8	$1/2^+$	799.18(10)	0.043(6)
302.8	$5/2^+$	302.54(6)	0.045(4)			359.395(25)	0.453(11)			966.16(11)	0.073(7)
312.2	$7/2^+$	312.00(11)	0.024(4)			604.58(14)	0.049(11)	1359.4	1/2,3/2	[224.717(7)]	[0.0040]
381.1	$3/2^+$	[266.1(2)]	[0.000001]	623.5	$1/2^+$	[189.920(3)]	[0.017]	1359.4	1/2,3/2	685.74(11)	0.16(3)
		381.81(11)	0.0034(5)			297.86(7)	0.072(6)			754.80(3)	0.179(7)
392.4	$7/2^+$	[80.1(3)]	[0.002]			[332.050(5)]	[0.018]			[1019.868(27)]	[0.084]
		392.41(15)	0.025(6)			[347.192(6)]	[0.011]	6153.5	$1/2^+$	4793.79(24)	0.42(4)
471.2	$(3/2)^+$	471.29(15)	0.024(5)			[357.148(9)]	[0.0036]			4920.2(3)	0.121(11)
670.1	$5/2^+$	[102.4(5)]	[0.0004]			623.1(3)	0.05(3)			5006.3(5)	0.045(11)
		[198.7(5)]	[0.0072]	673.5	$3/2^-$	333.944(24)	0.220(9)			5018.8(6)	0.054(11)
		[277.58(20)]	[0.023]			[346.622(6)]	[0.0019]			5100.1(6)	0.026(11)
		[288.28(20)]	[0.0096]			428.46(6)[c]	0.010(2)			5211.8(3)	0.231(19)
		[321.84(20)]	[0.030]			[673.607(40)]	[0.0035]			5432.0(5)	0.064(11)
		[357.84(20)]	[0.0054]	722.0	$3/2^+, 5/2$	230.60(18)	0.022(4)			5479.7(3)	0.055(9)
		[367.31(20)]	[0.025]			288.29(14)	0.018(4)			5719.4(3)	0.121(15)
		[554.4(3)]	[0.0010]			394.9(3)	0.025(7)			5829.0(3)	0.121(11)
		670.10(12)	0.029(4)			396.73(10)	0.087(11)			5887.2(7)	0.042(19)
^{109}Pd						455.72(8)	0.053(5)	^{111}Pd			
0	$5/2^+$					721.83(6)	0.087(7)	0	$5/2^+$		
113.4	$1/2^+$	113.47(3)	1.266(19)	791.4	$5/2^+, 3/2^+$	[365.295(7)]	[0.010]	191.3	$^+$	191.12(24)	0.033(9)
189.0	$11/2^-$	189.07(5)	0.103(6)			[464..541(9)]	[0.025]	195.1	$^+$	122.8(3)	0.021(13)
245.1	$7/2^-$,$5/2^-$	245.128(24)	0.945(15)			515.02(8)	0.090(8)			195.0	0.019(10)
248.0	$(9/2)^+$	59.4(3)	0.04(2)			[525.078(16)]	[0.023]	411.8	$7/2^+$,$9/2^+$	[136.4(3)]	[0.0035]
		247.96(11)	0.041(7)			[678.040(35)]	0.025]			[181.0(3)]	[0.0043]
266.3	$1/2^+$	152.99(3)	0.549(8)			791.12(20)	0.027(5)			[220.5(3)]	[0.0059]
		266.38(4)	0.195(4)	810.6	$3/2^+$	[187.115(4)]	0.0060]			412.3(4)	0.039(14)
276.3	$7/2^+$	276.31(3)	0.212(7)			377.004(13)	[0.010]	450.4	$3/2^-$,$5/2^-$	255.8(3)	0.016(12)
287.2	$9/2^-$	98.35(6)	0.082(6)			485.24(8)	0.046(5)			258.89(3)	0.0015(7)
291.4	$3/2^+$	178.11(3)	0.413(8)			810.42	0.083(11)				
		291.476(23)	0.393(8)	911.3	$5/2^+$	[584.505(51)]	[0.048]				
941.1	$3/2^-$	[267.610(5)]	[0.014]			586.8(4)	0.016(6)				
325.3	$3/2^+$	211.93(3)	0.204(7)			620.05(17)	0.052(9)				
		325.310(23)	0.786(11)			911.28(11)	0.040(5)				
326.9	$5/2^+$	326.88(4)	0.300(8)	941.1	$3/2^-$	[267.610(5)]	[0.014]				
339.5	$5/2^-$	94.50(5)	0.145(8)			336.64(4)	0.129(7)				
		339.526(21)	0.737(11)			601.56(5)	0.122(7)				
426.1	$7/2^+$	150.29(19)	0.0011(3)			[649.650(29)]	[0.0038]				

[a]Total cross section $\sigma_\gamma + \sigma_{\text{electron}}$ for $E0$ transition.

[c]Doublet intensity divided on the basis of literature branching ratios [7].

[b]Doublet intensity divided as discussed in text.

were allowed to fluctuate according to the Porter-Thomas distribution and varied between realizations.

A. Adopted models

The population of the low-lying levels depends on four factors: (i) level density, (ii) photon strength functions for different transition types ($M1$, $E1$, $E2$, ...), (iii) the experimental adopted level scheme below $E_{\rm cut}$, and (iv) the capture state spin composition, $J = J(\text{target}) \pm 1/2$, for odd- and odd-odd targets. There are large uncertainties in our knowledge of the first two factors and the experimental data may also be incomplete and uncertain. The experimental population of levels below $E_{\rm cut}$ and the capture state compositions can be compared to DICEBOX simulations for various formulations of each factor.

1. Level-density models

Two different models of level density were compared. The Constant Temperature Formula (CTF) in the form

$$\rho(E, J) = \frac{f(J)}{T} \exp\left(\frac{E - E_0}{T}\right), \tag{3}$$

and the back-shifted Fermi gas formula (BSFG) written as

$$\rho(E, J) = f(J) \frac{\exp\left(2\sqrt{a(E - E_1)}\right)}{12\sqrt{2}\sigma_c a^{1/4}(E - E_1)^{5/4}}. \tag{4}$$

Here, the spin distribution factor, $f(J)$ is given as [10]

$$f(J) = \frac{2J + 1}{2\sigma_c^2} \exp\left[-\frac{(J + 1/2)^2}{2\sigma_c^2}\right], \tag{5}$$

where σ_c is the spin cut-off parameter. Parameters T, E_0, a, and E_1 in Eqs. (3) and (4) are obtained by fitting the functional forms given by these equations to the experimental level densities below $E_{\rm cut}$ and the average spacing of neutron (proton) resonances near the capture state [11]. Adopted values of these parameters for the palladium isotopes are summarized in Table II.

The level density is usually assumed to be parity independent above $E_{\rm cut}$ but there are an excess of positive-parity levels below $E_{\rm cut}$ for all Pd isotopes. Although it is believed that the level density is parity-independent at high excitations there must be a transition to parity dependence at lower excitations. Al-Quraishi *et al.* [12] have proposed a parity-dependent level-density parametrization of this transition. This parametrization predicts a rapid onset of parity-independent level density at energies close to $E_{\rm cut}$ and has been ignored in these calculations.

2. Electric dipole strength models

Three models of PSFs were adopted for the dominant electric dipole ($E1$) transitions. The standard Lorentzian form, also called the Brink-Axel (BA) model [13,14], is written as

$$f_{\rm BA}^{(E1)}(E_\gamma) = \frac{1}{3(\pi\hbar c)^2} \frac{\sigma_G E_\gamma \Gamma_G^2}{\left(E_\gamma^2 - E_G^2\right)^2 + E_\gamma^2 \Gamma_G^2}, \tag{6}$$

where parameters E_G, Γ_G, and σ_G are the energy, width, and the cross section that describe the shape of $E1$ PSF near the maximum of the giant dipole electric resonance (GDER). We assume that $f^{(E1)}$ follows the Brink hypothesis [13] where the shape of the PSF does not depend on any quantum numbers of the initial and/or final states.

Two other models, one proposed by Kadmenskǐ, Markushev, and Furman (KMF) [15] for spherical nuclei, given as

$$f_{\rm KMF}^{(E1)}(E_\gamma, \Theta) = \frac{1}{3(\pi\hbar c)^2} F_K \frac{\sigma_G \Gamma_G E_G \Gamma_G(E_\gamma, \Theta)}{\left(E_\gamma^2 - E_G^2\right)^2}, \tag{7}$$

and another, proposed by Kopecky *et al.* [16,17], the generalized Lorentzian (GLO) model written as

$$f_{\rm GLO}^{(E1)}(E_\gamma, \Theta) = \frac{1}{3(\pi\hbar c)^2} \left[\frac{E_\gamma \Gamma_G(E_\gamma, \Theta)}{\left(E_\gamma^2 - E_G^2\right)^2 + E_\gamma^2 \Gamma_G^2(E_\gamma, \Theta)} + F_K \frac{4\pi^2\Theta^2\Gamma_G}{E_\gamma^5}\right] \sigma_G \Gamma_G, \tag{8}$$

depend on the γ-ray energy and the excitation energy of final state that is represented by the temperature Θ. Consequently these models partially violate the Brink hypothesis. The temperature-dependent width in the KMF and GLO models is given by

$$\Gamma_G(E_\gamma, \Theta) = \frac{\Gamma_G}{E_G^2}\left(E_\gamma^2 + 4\pi^2\Theta^2\right), \quad \Theta = \sqrt{(E - \Delta)/a}, \tag{9}$$

with E, Δ, and a the excitation energy of a final level, the pairing energy and the shell-model LD parameter, respectively. We set the factor F_K to 0.7 [15]. The KMF model results from microscopic calculations within the framework of the semimicroscopic shell-model approach based on the results of the theory of Fermi liquids. It was proposed as an approximation describing the behavior of the $E1$ PSF at the low-energy tail of the electric GDER of spherical nuclei. Nevertheless, it is often applied to somewhat nonspherical nuclei. Conversely the GLO model is purely phenomenological and reasonably describes the (n, γ) data in ^{106}Pd [16] as shown in Fig. 2. For deformed nuclei the GDER is split into two components and the PSF is given by a sum of two resonance terms on the right-hand sides of Eqs. (6) and (8).

Two sets of GDER parameters E_G, Γ_G, and σ_G were used in the palladium simulations. One is taken from the survey of Dietrich and Berman [18]. Their parameters $E_G =$

TABLE II. Level density [11], pairing, and deformation [19] parameters adopted in the palladium DICEBOX simulations.

Nucleus	T (MeV)	E_0 (MeV)	a (MeV^{-1})	E_1 (MeV)	Δ (MeV)	β_2
^{103}Pd[a]	0.804	−2.16	11.98	−0.88	1.24	0.196
^{105}Pd	0.804	−2.16	11.98	−0.88	1.18	0.209
^{106}Pd	0.753	−0.29	13.09	0.84	2.84	0.229
^{107}Pd	0.777	−2.30	12.40	−1.04	1.09	0.243
^{109}Pd	0.730	−2.40	13.60	−1.01	0.95	0.258
^{111}Pd	0.645	−1.85	15.11	−0.81	0.87	0.220

[a]No experimental resonance spacings were available for this nucleus. The level-density parameters were adopted from ^{105}Pd.

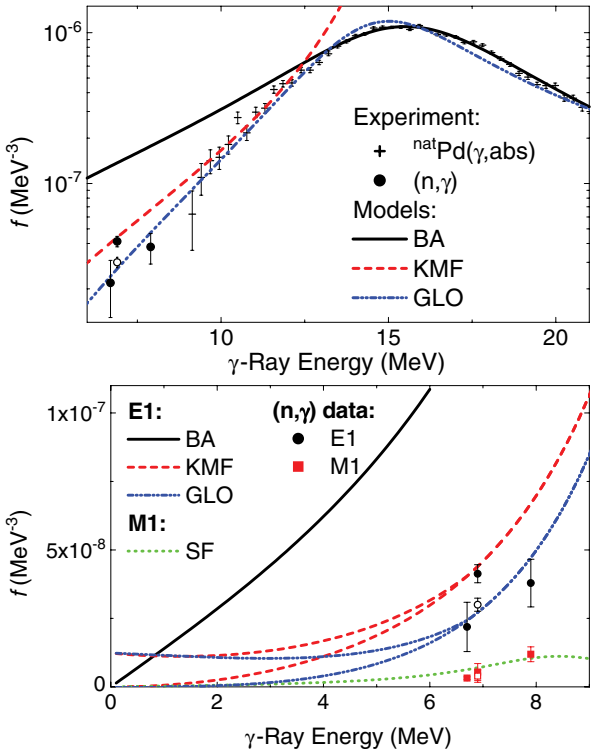

FIG. 2. (Color online) Shapes of different PSFs models for parameters of GDER from Dietrich and Berman [18]. Divergent curves for the temperature-dependent KMF and GLO models represent shapes of $f^{(E1)}$ for transitions to the ground state (lower curve) and from the neutron capturing state of ^{106}Pd (upper curve). Data for the (n,γ) reaction are from ^{104}Rh at 6.9 MeV [17], ^{106}Pd at 7.9 MeV [17] and ^{107}Ag at 6.7 MeV [19]. The recalculated values for ^{104}Rh (see text) are shown as open symbols. Photonuclear data are from the ^{nat}Pd(γ,n) reaction. The parameters for the M1 SF mode shown are $E_{SF} = 8.66$ MeV, $\Gamma_{SF} = 4.0$ MeV, and $\sigma_{SF} = 1.1$ MeV.

15.92 MeV, $\Gamma_G = 7.18$ MeV, and $\sigma_G = 199$ mb are based on the photonuclear data of Deague *et al.* [20] for a natural Pd sample. The unusually high value of the Γ_G in this parameter set may be due to a small deformation in the Pd isotopes (see Table II) splitting the GDER into two components. This splitting is not clearly pronounced in the experimental data, which were fit with a single Lorentzian [18]. The same GDER parameter set was used for all Pd isotopes as justified by the similar deformations for all Pd nuclei as shown in Table II. In Fig. 2 the energy dependence of the three models of $f^{(E1)}$ for this parametrization of GDER is compared to photonuclear data on ^{nat}Pd and (n, γ) data from this mass region.

A second set of GDER parameters were taken from the EMPIRE code systematics [21] (see Table III) that reflect the deformation of Pd isotopes by splitting the GDER into two components. The corresponding PSFs for the three different electric-dipole models are shown in Fig. 3.

As shown in Figs. 2 and 3, experimental data for γ-ray energies below $\approx$11 MeV disagree with the BA model but are more consistent with the KMF and GLO models [16]. The deviation of BA model from photonuclear data is seen for all available photonuclear data from $100 < A < 110$ nuclei, as shown in Fig. 4. The BA model of the E1 PSF at energies

TABLE III. Parameters of GDER deduced from EMPIRE database [22].

Nucleus	E_{G1}	Γ_{G1}	σ_{G1}	E_{G2}	Γ_{G2}	σ_{G2}
^{103}Pd	14.17	3.27	110	17.06	5.50	129
^{105}Pd	13.93	3.18	115	16.98	5.44	133
^{106}Pd	13.65	3.04	121	16.95	5.39	136
^{107}Pd	13.62	3.03	123	16.91	5.38	138
^{109}Pd	13.38	2.93	129	16.84	5.32	143
^{111}Pd	13.15	2.83	136	16.77	5.27	148

below the maximum of GDER is strongly disfavored in this mass region.

Primary transition intensities from thermal neutron capture, shown in Figs. 2–4, come from reactions on the three different nuclei. Data at 6.7 MeV are from ^{108}Ag [19], 6.9 MeV from ^{104}Rh [17], and at 7.9 MeV from ^{106}Pd [17]. An important quantity determining the absolute value of the PSF is the average spacing between s-wave resonances that is deduced from epithermal (n, γ) reactions. Recent experimental values of the resonance spacing in ^{106}Pd [22] and ^{108}Ag [23] are comparable to those used to derive the PSF, but the spacing for ^{104}Rh is very different. The values of PSFs for ^{104}Rh [17] were based on an average resonance s-wave spacing of 23.2 eV, which is lower than the value 28.2(15) eV recommended by Mughabghab [23]. The strength recalculated using this higher value is shown by the open symbols in Figs. 2–4.

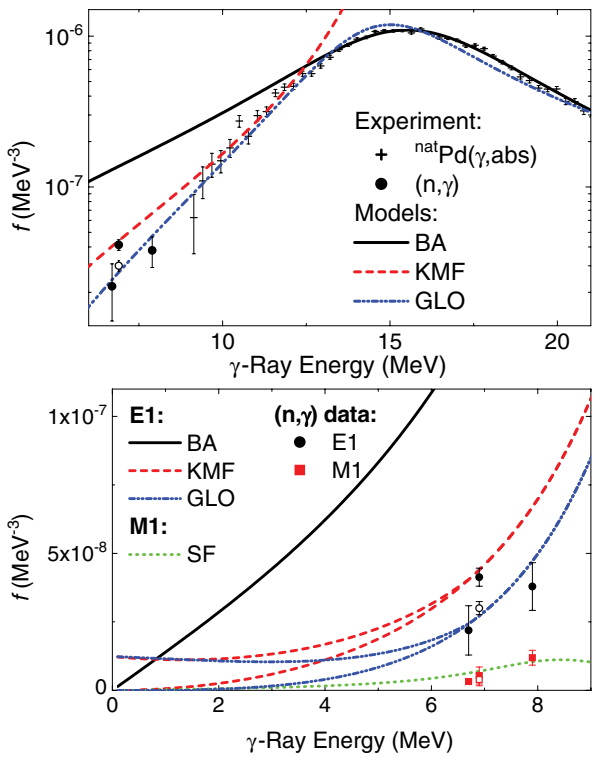

FIG. 3. (Color online) Shapes of different PSFs models for parameters of GDER for the parameter set from Ref. [21] for ^{106}Pd as described in the caption for Fig. 2.

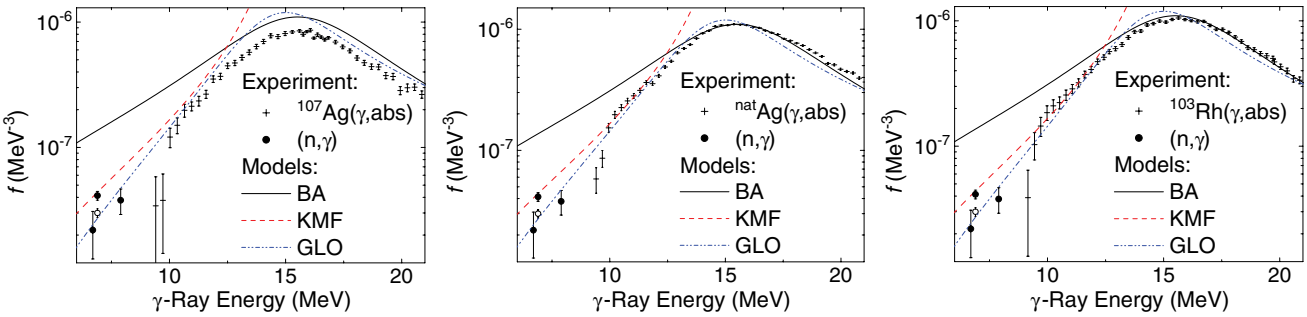

FIG. 4. (Color online) Comparison of E1 PSF obtained by fitting photonuclear data on ^{nat}Pd with other photonuclear data from neighboring nuclei.

3. *Magnetic dipole strength models*

Two models were compared for $M1$ transitions. The single-particle (SP) model $f^{(M1)}$ is an energy independent constant, and the spin-flip (SF) model can be described as a Lorentzian-shaped resonance peaked at ≈8.5 MeV with a width $\Gamma_{SF} \approx 4$ MeV [17]. This resonance corresponds to spin-flip transitions between neighboring shells and is plotted in Figs. 2 and 3. We note that few data are available for the $M1$ strength below about 6 MeV.

The absolute value of $M1$ PSF can be adjusted in various ways. One method is to fix $f^{(E1)}/f^{(M1)} \approx 5$–7 based on the systematics of nuclei with $A \gtrsim 100$ at about $E_\gamma = 7$ MeV [24]. Another method is to normalize the $M1$ strength to experimental (n,γ) cross-section data. Results from both approaches are reasonably consistent with the energy dependence of the KMF and GLO models for the $E1$ strength but disagree with BA model. In the simulations of the BA model we adjusted the $M1$ strength to $f^{(M1)} = 1.2 \times 10^{-8}$ MeV^{-3} at $E_\gamma \approx 7$ MeV, approximately corresponding to $f^{(E1)}/f^{(M1)} = 7$. The comparable values for $f^{(M1)}$ used with the KMF and GLO models were $f^{(M1)} = 0.3 \times 10^{-8}$ and 0.2×10^{-8} MeV^{-3}, respectively.

4. *Electric quadrupole strength*

For electric-quadrupole strength, which contributes far less than the dipole strengths, we used the single-particle model with a constant value $f_{SP}^{(E2)} = 5 \times 10^{-11}$ MeV^{-5}.

5. *Additional constraints on PSFs and level-density models*

PSFs for γ-ray energies below neutron binding energy are constrained by the total radiation width of the neutron resonances, Γ_γ^{tot}. Available experimental values of Γ_γ^{tot} from Ref. [23] are compared to simulated values obtained with several combinations of PSFs and level density (PSFs/LD combinations) in Table IV. The total radiation width is strongly dependent on the absolute values and energy dependencies of PSFs as well as on the shape of level density. For all models of PSF Γ_γ^{tot} is 50–80% greater for the BSFG level density model than for the CTF model. Uncertainties shown in

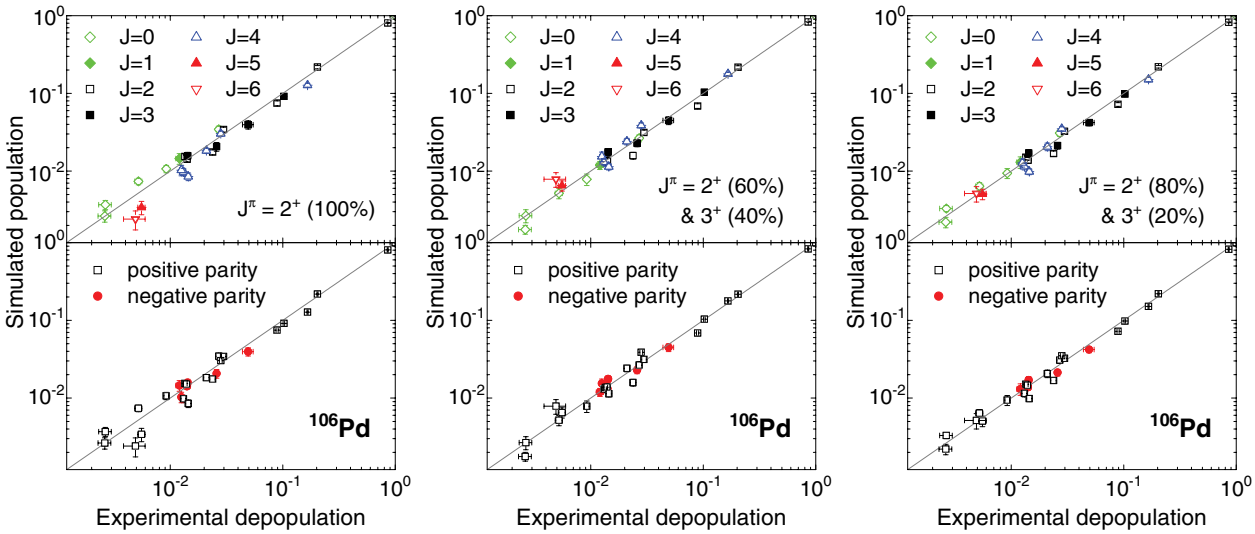

FIG. 5. (Color online) Population-depopulation balance of low-lying levels in ^{106}Pd for different composition of capturing spin. Combination (KMF+SP)/BSFG was used for PSFs/LD with $E1$ parametrization from Ref. [21]. The difference is most apparent for low- ($J = 0, 1$) and high- ($J = 5, 6$) spin states.

TABLE IV. Simulated values of total radiation widths of Pd isotopes for various combinations of PSFs and level density. Values for two sets of GDER parameters are shown, see text. For explanation of bold numbers see text too.

Isotope	$E1$	$M1$	LD	$\Gamma_\gamma^{\rm tot}$ (meV)	
				$E1$ from Ref. [18]	$E1$ from Ref. [21]
			Experiment 148(10)		
^{105}Pd	BA	SP	CTF	410(47)	253(23)
	BA	SF	CTF	352(42)	184(24)
	KMF	SP	BSFG	201(14)	**123(9)**
	KMF	SF	BSFG	172(12)	105(8)
	GLO	SP	BSFG	**156(8)**	101(6)
	GLO	SF	BSFG	126(8)	82(5)
			Experiment 151(5)		
^{106}Pd	BA	SP	CTF	316(7)	198(4)
	BA	SF	CTF	263(7)	143(4)
	KMF	SP	BSFG	211(3)	**135(2)**
	KMF	SF	BSFG	183(3)	98(2)
	GLO	SP	BSFG	**170(3)**	116(2)
	GLO	SF	BSFG	143(2)	83(2)
			Experiment 77(5)		
^{109}Pd	BA	SP	CTF	247(22)	160(13)
	BA	SF	CTF	202(21)	115(12)
	KMF	SP	BSFG	98(5)	**67(3)**
	KMF	SF	BSFG	85(5)	52(3)
	GLO	SP	BSFG	**75(3)**	53(3)
	GLO	SF	BSFG	61(3)	39(2)
			Experiment 56(3)		
^{111}Pd	BA	SP	CTF	139(10)	94(6)
	BA	SF	CTF	110(10)	65(5)
	KMF	SP	BSFG	64(3)	**48(3)**
	KMF	SF	BSFG	49(3)	32(2)
	GLO	SP	BSFG	**50(2)**	39(2)
	GLO	SF	BSFG	36(2)	25(2)

Table IV represent fluctuations between the different nuclear realizations. The experimental values of $\Gamma_\gamma^{\rm tot}$ are reasonably reproduced with the same sets of models in all nuclei. We emphasize that $\Gamma_\gamma^{\rm tot}$ is the only simulated quantity that depends on the absolute values of PSFs. If all PSFs were multiplied by a constant factor the simulated $\Gamma_\gamma^{\rm tot}$ would be multiplied by the same factor while the populations of low-lying levels would remain exactly the same.

Analysis of the population of low-lying levels following radiative neutron capture on isolated resonances together with data from two-step cascade (TSC) measurements in ^{108}Ag [19] indicates that the $f^{(E1)}$ and $f^{(M1)}$ are comparable for γ-ray energies of $\approx$3 MeV in this mass region. This is consistent with use of the SP model for $M1$ PSF but inconsistent with pure SF models.

Combining all restrictions on the PSFs, the preferred model combinations for the palladium simulations are KMF with parametrization from Ref. [21] or GLO with parametrization from Ref. [18] models for $E1$, the SP model for $M1$, and the BSFG level-density formula. However, simulations were performed for four other PSFs/LD combinations and also for both adopted parametrizations of $E1$ PSF. Values corresponding to preferred models are given in bold in Table IV.

IV. RESULTS

The total radiative (n,γ) cross section σ_0 is defined by the sum of transition cross sections populating the ground state $\Sigma\sigma_\gamma$(GS) from all levels, which is identical to the sum of primary γ-ray cross sections $\Sigma\sigma_\gamma$(cap) de-exciting the capture state. For all other levels the sum of γ-ray cross sections populating a level equals the sum of γ-ray cross sections depopulating that level. The observed cross section populating the GS is usually incomplete for high-Z isotopes and must be supplemented by the simulated population from all other levels. Simulations predict the population of low-lying levels per neutron capture and must be renormalized to convert them to cross sections. If σ_γ(GS) is completely known for all levels

below E_{cut} from experiment, as is the case for ^{106}Pd and ^{109}Pd, this is done by renormalizing the simulated population of all levels below E_{cut} to the measured cross section de-exciting those levels to the GS. If the cross sections de-exciting levels below E_{cut} are not all measured, the simulated populations can be normalized independently for each level for which the depopulation intensity is known. Then σ_0 can be calculated from the renormalized simulated cross section feeding the ground state and the results from each level averaged to give a final adopted value for σ_0.

Comparison of experiment and simulation for individual levels can be visualized by plotting the experimental depopulation of levels below E_{cut} against their simulated populations in population-depopulation (P-D) diagrams. If the simulation is correct, all points in these diagrams should align with the slope giving the normalization of the simulation from transition intensity per neutron capture to the experimental cross section. Scatter around the line indicates the quality and completeness of both the simulation and the experimental data. In principle, these diagrams can be easily used to dividing intensity of an unresolved measured doublet as it was done in ^{106}Pd, see below. Uncertainties in these diagrams along the horizontal axis correspond to experimental errors while those along the vertical axis come from uncertainties due to Porter-Thomas fluctuations while generating partial radiation widths and level scheme in different nuclear realizations.

A. ^{105}Pd$(n,\gamma)^{106}$Pd

γ-ray radiative cross sections σ_γ de-exciting levels up to 3.25 MeV in ^{106}Pd are given in Table I. The ^{106}Pd level scheme has been taken from ENSDF [25]. It is well known and likely to be complete up to $E_{cut} = 2.51$ MeV. We removed the 1904-keV level reported in ENSDF, reassigning the γ rays from that level to the 1909-keV level on the basis of energy sums. This change is supported by simulations indicating that a level at 1904 keV with $J^\pi = (2^-, 3^-)$ would be much more intensely populated than was suggested. The intensities of a 848.11-keV γ-ray doublet de-exciting levels at 2076.3 keV (6^+) and 2076.6 keV (4^+) were divided on the bases of our statistical model calculations predicting much more intense population of levels with $J^\pi = 4^+$ than $J^\pi = 6^+$ levels. A total of 26 levels with spins ranging $0 \leqslant J \leqslant 6$ known below E_{cut} were used in these simulations. The thermal radiative neutron capture γ-ray cross section depopulating each of the levels below E_{cut}, which equals the cross section populating it, can be determined from the σ_γ in Table I.

For ^{105}Pd(n,γ) the target ground state is $J^\pi = 5/2^+$ and the ^{106}Pd capture state is $J^\pi = 2^+, 3^+$. The "completeness" of the ^{106}Pd neutron capture decay scheme below E_{cut} makes this nucleus an excellent case to test model dependence of simulated populations of low-lying levels on different spin composition of capturing. This is evident because the $J = 2^+$ component favors the population of the the lower spin levels with $J = 0, 1$ and the $J = 3^+$ component favors population of the higher spin levels with $J = 5, 6$. The relative contribution of $J^\pi = 2^+, 3^+$ capture state spins can be parameterized by the ratio $R_J = I_L/I_H$, where I_L is the depopulation intensity of all $J = 0$ and 1 excited states below E_{cut} and I_H is the depopulation intensity of all $J = 5$ and 6 levels. The experimental value $R_J = 5.6 \pm 0.6$ has been compared with simulated values for various contributions of capture state spins shown in Table V and indicates that $J = 2$ resonances are populated by 70–80% of the total neutron capture cross section. This is also seen in (P-D) diagrams (see Fig. 5) comparing experimental and simulated ^{106}Pd level feeding assuming $J^\pi = 2^+$, $J^\pi = 2^+(80\%) + 3^+(20\%)$, and $J^\pi = 2^+(60\%) + 3^+(40\%)$ capture states. Our value is consistent with an 87% contribution from $J = 2$ resonances calculated from resonance data [23]. Thermal neutron capture is dominated by bound (negative) resonances in this nucleus and it is not easy to accurately separate the contribution of bound resonances with different spins.

TABLE V. Simulated values of R_J, see text, as a function of the ratio of 2^+ to $(2^+ + 3^+)$ composition of capturing state for the ^{106}Pd. The experimental value is $R_J^{(exp)} = 5.6(6)$.

Model	Capture state $2^+/(2^+ + 3^+)$ ratio				
	0.6	0.7	0.8	0.9	1.0
(GLO+SP)/BSFG	3.6(7)	4.6(7)	5.6(8)	7.5(11)	11.1(18)
(KMF+SP)/BSFG	3.9(6)	5.0(7)	6.4(9)	8.3(13)	12.6(21)

Figure 6 shows (P-D) diagrams for various $M1$ PSF models assuming the fraction of capture state resonances F_J with $J^\pi = 2^+$ is 0.8. The best fit favors the SP model for $M1$ with $f_{SP}^{(M1)} \approx 2 \times 10^{-9}$ MeV^{-3}. As discussed above this value was used in simulations. The (P-D) diagrams in Figs. 5 and 6 indicate that the statistical model is applicable for simulating the population of low-lying levels in ^{106}Pd. Trend lines for different spins and/or parities of low-lying states in (P-D) diagrams vary due to deficiencies in the (PSFs/LD) models.

Predicted direct feeding of the ground state from levels above E_{cut} (GS sidefeeding) for six different PSFs/LD models is tabulated in Table VI. Bold values in the table indicate our preferred model combinations, see Sec. III A5, which yielded 8.0(15)% GS sidefeeding, which combined with

TABLE VI. GS sidefeeding of ^{106}Pd as predicted by the DICEBOX simulations for different model combinations of PSFs and level density. The factor F_J gives the relative contribution of resonances with $J^\pi = 2^+$ to total cross section. Values in bold were averaged to give an adopted sidefeeding of 8.0(15)%.

$E1$	$M1$	LD	F_J	GS sidefeeding (%)	
				$E1$ from Ref. [18]	$E1$ from Ref. [21]
BA	SP	CTF	0.8	4.6(6)	5.2(9)
BA	SF	CTF	0.8	5.6(8)	6.1(11)
KMF	SF	BSFG	0.8	7.3(6)	7.4(8)
KMF	SP	BSFG	0.7	6.7(7)	**6.9(9)**
KMF	SP	BSFG	0.8	7.7(10)	**7.6(10)**
GLO	SP	BSFG	0.7	**8.0(9)**	8.0(10)
GLO	SP	BSFG	0.8	**8.7(12)**	8.7(11)
GLO	SF	BSFG	0.8	8.2(7)	8.2(7)

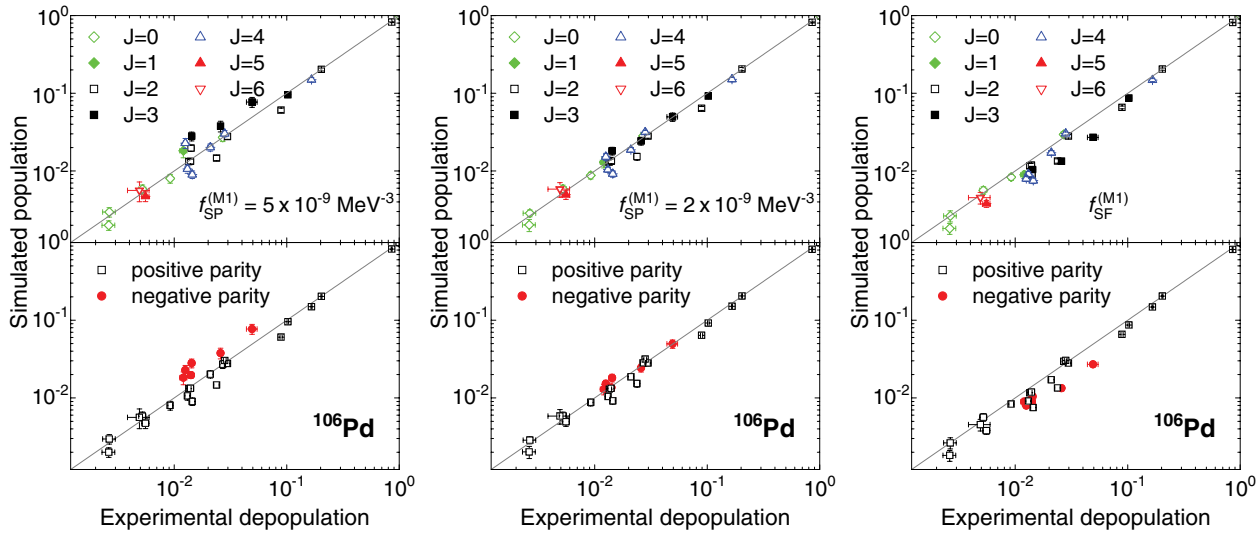

FIG. 6. (Color online) Population-depopulation balance of low-lying levels in ^{106}Pd for different $M1$ PSFs models in the combination with GLO model for $E1$ with parameter set from Ref. [18]. From left to right, $f_{SP}^{(M1)} = 0.5$ MeV^{-3}, $f_{SP}^{(M1)} = 0.2$ MeV^{-3}, $f_{SF}^{(M1)}$.

the measured ground-state feeding from levels below E_{cut} gives $\sigma_0 = 21.7(5)$ b. This value is in excellent agreement with $\sigma_0 = 21.0(15)$ b, which was adopted by Mughabghab [23].

B. ^{108}Pd$(n,\gamma)^{109}$Pd

For ^{109}Pd, below the energy $E_{cut} = 350$ keV, 12 levels with $1/2 \leqslant J \leqslant 11/2$ are known. This value of E_{cut}, is much lower than for the even-even ^{106}Pd, which is typical for odd-A nuclei where the pairing gap is zero. The percentage of GS sidefeeding from levels above E_{cut} in ^{109}Pd is given in Table VII for various model combinations. A (P-D) diagram comparing the simulated population of levels below E_{cut} for the favored (KMF+SP)/BSFG combination is compared with experimental values in Fig. 7. From the preferred PSFs/LD model calculations shown in bold in Table VI, the simulated GS sidefeeding from levels above E_{cut} is 18(6)%, which combined with the measured ground-state feeding from levels below E_{cut} gives $\sigma_0 = 7.2(5)$ b for ^{108}Pd. This value is in excellent agreement $\sigma_0 = 7.6(5)$ b, which was adopted by Mughabghab [23]. The cross section $\sigma_0 = 0.185(11)$ b populating the 189-keV, $J^\pi = 11/2^-, t_{1/2} = 4.7$ m isomer ^{109m}Pd was directly measured in this work and is nearly identical to 0.185(10) b adopted by Mughabghab [23]. As shown in Fig. 7, the simulated population of this isomer is consistent with experiment.

TABLE VII. GS sidefeeding to ^{109}Pd as predicted by the DICEBOX simulations for different model combinations of PSFs and level density. Values in bold were averaged to give an adopted GS sidefeeding of 18(6)%.

$E1$	$M1$	LD	GS sidefeeding (%)	
			$E1$ from Ref. [18]	$E1$ from Ref. [21]
BA	SP	CTF	24.8(51)	24.5(49)
BA	SF	CTF	25.2(49)	25.8(48)
KMF	SP	BSFG	22.4(48)	**21.0(47)**
KMF	SF	BSFG	27.8(43)	28.0(42)
GLO	SP	BSFG	**16.6(44)**	16.9(42)
GLO	SF	BSFG	26.5(40)	25.3(41)

C. ^{102}Pd$(n,\gamma)^{103}$Pd

The ^{103}Pd level scheme is poorly characterized and the intensity of only two ground-state transitions de-exciting levels at 118.7 and 504.2 keV were measured in this nucleus. There are three additional levels known at 244.0-keV ($7/2^+$), 266.9-keV ($5/2^+$), and 498.0-keV ($1/2^+$) that were not observed in this experiment below 510 keV. It is very likely that other low-spin levels exist below 510 keV, e.g., there are six known levels between 300 and 500 keV in ^{109}Pd. To assess the affect of an incomplete level scheme we made simulations with $E_{cut} = 270$ keV and $E_{cut} = 510$ keV. The populations of low-lying levels from these simulations are summarized in Table VIII, where they show two interesting features: (i) populations calculated with two different E_{cut} are consistent and (ii) those obtained with lower E_{cut} display stronger fluctuations as expected if less of the level scheme is specified. It is reassuring that the σ_0 values are only weakly dependent on E_{cut}.

The experimental cross section de-exciting the 504.2-keV level is much larger than is suggested by the simulated feeding, indicating that either that level is populated by an unusually intense primary γ ray or the 385.4-keV γ-ray intensity de-exciting the level includes a large impurity from an unknown source. We adopted populations obtained with the lower value of E_{cut} for determining the σ_0 because incompleteness of the level scheme for higher E_{cut} choices may influence the

TABLE VIII. Percentage population of 119- and 504-keV levels in ^{103}Pd as predicted by the DICEBOX simulations for different model combinations of PSFs and level density. Values in bold were averaged to obtain an adopted level population of 47(14)%.

$E1$	$M1$	LD	E_{cut} (keV)	$E1$ from Ref. [18]		$E1$ from Ref. [21]	
				119	504	119	504
BA	SP	CTF	270	49(9)		48(10)	
			510	60(6)	11.7(21)	59(5)	11.0(20)
BA	SF	CTF	270	46(10)		48(10)	
			510	57(7)	10.2(17)	58(5)	10.7(17)
KMF	SP	BSFG	270	51(9)		**49(10)**	
			510	58(4)	9.3(19)	54(5)	8.4(19)
KMF	SF	BSFG	270	49(7)		49(8)	
			510	56(4)	9.3(16)	55(4)	8.9(16)
GLO	SP	BSFG	270	**46(12)**		44(13)	
			510	53(5)	7.6(17)	50(6)	6.9(16)
GLO	SF	BSFG	270	47(8)		43(8)	
			510	55(3)	8.3(14)	52(4)	7.4(13)

simulated population of low-lying levels. This approach was also applied to other palladium isotopes. Using our preferred choices of PSFs/LD and $E_{cut} = 270$ keV, the simulated feeding of the 118-keV level is 47(14)% corresponding to $\sigma_0 =$ 1.1(4) b. This value is slightly lower than $\sigma_0 = 1.82(20)$ b measured by Duncan and Krane [26] that was adopted by Mughabghab [23]. That result assumed an adopted transition probability for the 357.4-keV γ ray from ^{103}Pd decay of $P_\gamma = 0.000221(7)$ [27], which was superseded by a newer value $P_\gamma = 0.000245(8)$ [28]. Renormalizing Mughabghab's recommended value gives $\sigma_0 = 1.6(2)$ b, which is in better agreement with our measurement.

D. ^{104}Pd$(n, \gamma)^{105}$Pd

We observed γ rays de-exciting five levels below 500 keV in ^{105}Pd. Additional levels below 500 keV are known at 319.2-keV $(5/2^+)$, 447 keV $(3/2^+, 5/2^+)$, whose γ-ray de-excitations are unknown, and 489.14-keV $(11/2^-)$. Simulations were performed for various combinations of PSFs and level densities at two different critical energies, $E_{cut} =$ 350 keV and 500 keV. The results of these simulations are shown in Table IX. Variations in the average level populations for the two E_{cut} values again agree within uncertainty irrespective of the combination of PSFs and level density chosen. The total radiative cross section for ^{104}Pd, independently calculated from the depopulation cross sections of the 280-, 306-, and 344-keV levels, is internally consistent leading to an average total radiative cross section $\sigma_0 = 0.75(26)$ b, which is in excellent agreement with $\sigma_0 = 0.65(30)$ b recommended by Mughabghab [23].

E. ^{106}Pd$(n, \gamma)^{107}$Pd

γ-ray cross sections were measured de-exciting five levels in ^{107}Pd with energies below 400 keV. Three additional levels are known below this energy at 214.6 keV $(11/2^-)$, 348.2 keV (J^π unknown), and 366.8 keV $(7/2^+)$ but were not observed in this work. We compared the feeding of low-lying levels

TABLE IX. Percentage population of levels in ^{105}Pd predicted by DICEBOX simulations for different model combinations of PSFs and level density. Values in bold were averaged to obtain adopted level populations of 4.2(13)% to the 306-keV level and 10(3)% to the 344-keV level.

$E1$	$M1$	LD	E_{cut} (keV)	$E1$ from Ref. [18]				$E1$ from Ref. [21]			
				280	306	344	442	280	306	344	442
BA	SP	CTF	350	32(7)	3.1(12)	18(5)		31(7)	3.5(13)	18(5)	
BA	SP	CTF	500	36(5)	4.1(16)	22(4)	2.1(8)	36(5)	4.4(16)	21(5)	2.4(8)
BA	SF	CTF	350	30(6)	2.2(9)	18(6)		30(7)	2.4(9)	17(6)	
KMF	SP	BSFG	350	26(8)	3.8(11)	12(3)		**26(9)**	**4.1(12)**	**10(3)**	
KMF	SP	BSFG	500	32(6)	4.8(12)	17(4)	2.1(5)	32(6)	5.2(14)	16(4)	2.3(5)
KMF	SF	BSFG	350	29(6)	3.5(9)	14(3)		28(6)	4.1(9)	13(3)	
GLO	SP	BSFG	350	**23(9)**	**4.3(13)**	**10(3)**		25(10)	4.4(20)	10(3)	
GLO	SP	BSFG	500	29(8)	5.2(20)	14(5)	2.0(5)	28(8)	5.2(19)	14(5)	2.3(5)
GLO	SF	BSFG	350	25(8)	3.9(8)	11(3)		24(8)	4.6(9)	10(3)	

TABLE X. Percentage population of levels in ^{107}Pd predicted by DICEBOX simulations for different model combinations of PSFs and level density. Values in bold were averaged to obtain adopted level populations of 33(12)% to the 116-keV level, 10(4)% to the 303-keV level, and 3.9(14)% to the 312-keV level.

$E1$	$M1$	LD	E_{cut}	$E1$ from Ref. [18]					$E1$ from Ref. [21]				
			(keV)	116	303	312	382	392	116	303	312	382	392
BA	SP	CTF	330	41(7)	13(4)	3.9(27)			40(8)	12(4)	4.1(26)		
BA	SP	CTF	400	35(7)	9.9(19)	2.3(10)	13(3)	1.5(4)	34(7)	9.7(18)	2.5(11)	12.2(23)	1.6(3)
BA	SF	CTF	330	40(7)	11(4)	2.4(9)			39(8)	11(4)	2.5(9)		
BA	SF	CTF	400	36(7)	8.8(16)	1.7(10)	12(3)	0.8(2)	35(7)	9.0(15)	1.8(9)	12(3)	1.0(3)
KMF	SP	BSFG	330	36(10)	9.9(36)	3.6(13)			**35(10)**	**10(4)**	**3.9(14)**		
KMF	SP	BSFG	400	32(9)	8.2(22)	2.6(13)	9.9(18)	1.5(5)	33(4)	6.2(11)	2.5(8)	9.9(8)	1.6(7)
KMF	SP	CTF	330	37(10)	11(3)	3.6(21)			36(11)	11(4)	3.9(21)		
KMF	SF	BSFG	330	36(7)	11(3)	3.2(10)			34(6)	11(3)	3.6(10)		
GLO	SP	BSFG	330	**31(11)**	**9.0(40)**	**3.8(12)**			33(11)	10(4)	4.0(15)		
GLO	SP	BSFG	400	28(11)	7.0(21)	2.4(9)	8.4(13)	1.4(3)	29(10)	7.7(20)	2.5(9)	9.6(15)	1.5(4)
GLO	SP	CTF	330	34(14)	9.3(30)	3.6(20)			35(13)	10(3)	3.8(20)		
GLO	SF	BSFG	330	32(6)	9.9(24)	3.9(10)			30(7)	9.6(26)	3.8(10)		
GLO	SF	CTF	330	34(7)	9.7(25)	3.7(9)			32(8)	9.7(28)	3.6(9)		

for values of $E_{cut} = 330$ keV and 400 keV. The results of populations for different PSFs/LD combinations are shown in Table X. Total radiative cross sections for ^{104}Pd calculated independently from the depopulation cross sections of the 116-, 303-, and 312-keV levels were internally consistent, leading to an average measured radiative cross section $\sigma_0 = 0.36(10)$ b, which is in excellent agreement with the value $\sigma_0 = 0.30(3)$ b recommended by Mughabghab [23].

F. ^{110}Pd$(n, \gamma)^{111}$Pd

Only two prompt γ rays populating the $5/2^+$ ground state of ^{111}Pd ($t_{1/2} = 23.4$ m) were observed in this work. The ^{111}Pd level scheme is less well known than the other Pd isotopes. Definite spins and parities are known for only three levels below $E_{cut} = 200$ keV at $0(5/2^+)$, 72.2 keV $(1/2^+)$, and 172.2 keV $(11/2^-)$. Experimental σ_γ were measured depopulating two positive-parity levels of unknown spin at 191.3 and 195.1 keV. Simulations were restricted to two preferred PSF/LD combinations for spins from $J = 1/2$-$5/2^+$ for these two levels. The results are shown in Table XI. We found that the simulated population of these levels was relatively insensitive to the choice of J^π. The total radiative cross section populating ^{111}Pd ($t_{1/2} = 23.4$ m), calculated from the total depopulation cross section for the 191- and 195-keV levels is $\sigma_0 = 0.34(10)$ b, which is lower than $\sigma_0 = 0.70(17)$ b recommended

TABLE XI. Dependence of simulated level populations in ^{111}Pd assuming two preferred parameterizations and $J^\pi = 1/2$–$5/2^+$.

$E1$	$M1$	LD	J^π		Level feeding (%)	
$E1$ from Ref. [21]			191 keV	195 keV	191	195
KMF	SP	BSFG	$1/2^+$	$1/2^+$	11(3)	11(3)
KMF	SP	BSFG	$3/2^+$	$1/2^+$	15(3)	11(3)
KMF	SP	BSFG	$5/2^+$	$1/2^+$	11(3)	12(3)
KMF	SP	BSFG	$1/2^+$	$3/2^+$	11(3)	15(3)
KMF	SP	BSFG	$3/2^+$	$3/2^+$	15(4)	14(3)
KMF	SP	BSFG	$5/2^+$	$3/2^+$	11(3)	15(4)
$E1$ from Ref. [18]			191 keV	195 keV	191	195
GLO	SP	BSFG	$1/2^+$	$1/2^+$	9.3(25)	9.2(27)
GLO	SP	BSFG	$3/2^+$	$1/2^+$	13(3)	9.2(26)
GLO	SP	BSFG	$5/2^+$	$1/2^+$	10(3)	10.0(24)
GLO	SP	BSFG	$1/2^+$	$3/2^+$	9.3(26)	13(3)
GLO	SP	BSFG	$3/2^+$	$3/2^+$	13(4)	13(4)
GLO	SP	BSFG	$5/2^+$	$3/2^+$	9.2(25)	13(3)

TABLE XII. Total radiative thermal neutron capture cross sections σ_0 determined from measured transition cross sections σ_γ, corrected for internal conversion, and simulated level feedings calculated with the DICEBOX code.

Product isotope (J^π)	E (keV)	σ_γ(GS) (b)	Feeding (%)	σ_0[a] (b)	σ_0[b] (b)
^{103}Pd($3/2^+$)	119	0.52(14)	47(14)	1.1(4)	1.6(2)[c]
^{105}Pd($3/2^+$)	280	0.145(13)	24(11)	0.6(3)	
^{105}Pd($7/2^+$)	306	0.040(8)	4.2(13)	1.0(4)	
^{105}Pd($1/2^+$)	344	0.099(18)	10(3)	1.0(3)	
^{105}Pd	Sum	0.284(24)	38(13)	0.75(26)	0.65(30)
^{106}Pd(0^+)	$\leqslant$2500	20.0(3)	92.0(15)	21.7(5)	21.0(15)
^{107}Pd($1/2^+$)	116	0.095(9)	33(12)	0.29(11)	
^{107}Pd($5/2^+$)	303	0.046(4)	10(4)	0.46(20)	
^{107}Pd($7/2^+$)	312	0.024(4)	3.9(14)	0.62(24)	
^{107}Pd	Sum	0.165(11)	46(13)	0.36(10)	0.30(3)
^{109}Pd($5/2^+$)	$\leqslant$350	5.93(8)	82(6)	7.2(5)	7.6(5)
^{109m}Pd($11/2^-$)	189	0.185(11)		0.185(11)	0.185(10)
^{111}Pd(+)	191	0.035(10)			
^{111}Pd(+)	195	0.046(19)			
^{111}Pd	Sum	0.081(21)	24(4)	0.34(10)	0.70(17)

[a]This work.
[b]From Mughabghab [23] except as noted.
[c]From Ref. [26], re-evaluated as described in the text.

by Mughabghab [24] but comparable to $\sigma_0 = 0.39(8)$ b measured by Seren *et al*. [29].

V. CONCLUSIONS

We have developed a new method for determining total radiative thermal neutron cross sections σ_0 when the γ-ray cross-section yields from only a few transitions are known and the neutron capture decay scheme is incomplete. This method is based on the comparison of experimental transition cross sections depopulating low-lying levels with Monte Carlo simulations of their populations with the computer code DICEBOX. This code applies standard statistical model level densities and photon strength functions to generate multiple realizations of the neutron capture decay scheme that allow us to determine the statistical uncertainty in predicted populations. Calculated relative feeding of low-lying levels from thermal neutron capture is normalized to the experimental cross sections of γ rays de-exciting those levels to determine the unobserved cross section. This method is not restricted to thermal neutron cross sections but is applicable at any neutron energy assuming that the depopulation cross sections for low-lying states are known.

In this article we have demonstrated the applicability of our method for the six isotopes of palladium comparing γ-ray cross-section yields measured with the thermal neutron beam at the Budapest Reactor with DICEBOX calculations. These results, summarized in Table XII, are consistent with literature values, even when only one γ-ray cross section was measured and the level scheme was incomplete. Precision γ-ray cross-section measurements were performed at the Budapest Reactor for all stable elemental targets, and the method we developed can be applied to determine many additional total radiative neutron cross sections from existing data that were measured with a pure thermal neutron beam.

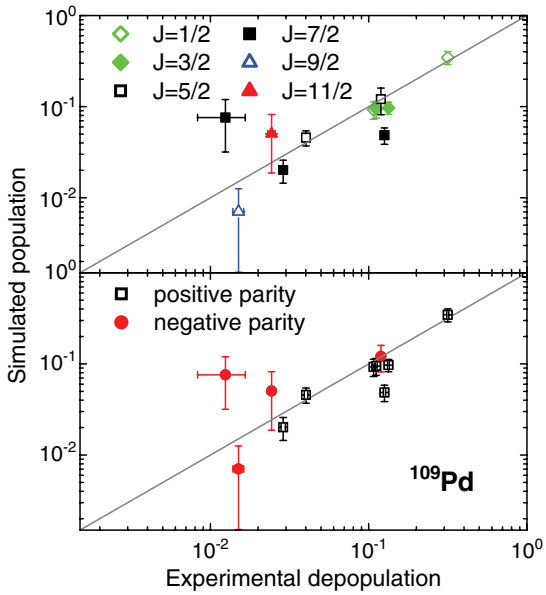

FIG. 7. (Color online) Population-depopulation balance for low-lying levels in ^{109}Pd obtained with (KMF+SP)/BSFG model combination with $E1$ parameters from Ref. [21].

ACKNOWLEDGMENTS

This work was performed under the auspices of the U.S. Department of Energy by the University of California, supported by the Director, Office of Science, Office of Basic Energy

Sciences, of the U.S. Department of Energy at Lawrence Berkeley National Laboratory under Contract No. DE-AC02-05CH11231 and at Lawrence Livermore National Laboratory under Contract W-7405-Eng-48. Support was also provided by National Nuclear Security Administration Academic Alliance Grant No. DE-FG52-06NA26194 and by the research plan MSM 002 162 0859 supplied by the Ministry of Education of the Czech Republic.

[1] F. Bečvář, Nucl. Instrum. Methods A **417**, 434 (1998).
[2] T. Belgya, Zs. Révay, B. Fazekas, I. Héjja, L. Dabolczi, G. L. Molnár, Z. Kis, J. Östör, and Gy. Kaszás, in *Proceedings of the 9th International Symposium on Capture Gamma-Ray Spectroscopy and Related Topics*, Budapest, Hungary, Oct. 8–12, edited by G. Molnár, T. Belgya, Zs. Révay (Springer-Verlag, Budapest/Berlin/Heidelberg, 1997), p. 826.
[3] Zs. Revay, T. Belgya, R. M. Lindstrom, Ch. Yonezawa, D. L. Anderson, Zs. Kasztovsky, and R. B. Firestone, *Handbook of Prompt Gamma Activations Analysis with Neutron Beams*, edited by G. L. Molnár (Kluwer, Boston, 2004).
[4] G. L. Molnár, Zs. Révay, and T. Belgya, Nucl. Instrum. Methods A **489**, 140 (2002).
[5] B. Fazekas, J. Östör, Z. Kis, G. L. Molnár, and A. Simonits, in *Proceedings of the 9th International Symposium on Capture Gamma-Ray Spectroscopy and Related Topics*, Budapest, Hungary, Oct. 8–12, edited by G. Molnár, T. Belgya, and Zs. Révay (Springer-Verlag, Budapest/Berlin/Heidelberg, 1997), p. 774.
[6] Zs. Révay and G. L. Molnár, Radiochim. Acta **91**, 361 (2003).
[7] Evaluated Nuclear Structure Data File, a computer file of evaluated experimental nuclear structure data maintained by the National Nuclear Data Center, Brookhaven National Laboratory.
[8] N. Bohr, Nature (London) **137**, 344 (1936).
[9] C. E. Porter and R. G. Thomas, Phys. Rev. **104**, 483 (1956).
[10] A. Gilbert and A. G. W. Cameron, Can. J. Phys. **43**, 1446 (1965).
[11] T. von Egidy, H. H. Schmidt, and A. N. Behkami, Nucl. Phys. **A481**, 189 (1988).
[12] S. I. Al-Quraishi, S. M. Grimes, T. N. Massey, and D. A. Resler, Phys. Rev. C **67**, 015803 (2003).
[13] D. M. Brink, Ph.D. thesis, Oxford University, 1955.
[14] P. Axel, Phys. Rev. **126**, 671 (1962).
[15] S. G. Kadmenskiĭ, V. P. Markushev, and V. I. Furman, Yad. Fiz. **37**, 277 (1983), [Sov. J. Nucl. Phys. **37**, 165 (1983)].
[16] J. Kopecky and M. Uhl, Phys. Rev. C **41**, 1941 (1990).
[17] R. B. Firestone, H. D. Choi, R. M. Lindstrom, G. L. Molnar, S. F. Mughabghab, R. Paviotti-Corcuera, Zs. Revay, V. Zerkin, and C. M. Zhou, Database of Prompt Gamma Rays from Slow Neutron Capture for Elemental Analysis, IAEA STI/PUB/1263 (2007), pp 251.
[18] S. S. Dietrich and B. L. Berman, At. Data Nucl. Data Tables **38**, 199 (1988).
[19] L. Zanini, F. Corvi, H. Postma, F. Becvar, M. Krticka, J. Honzatko, and I. Tomandl, Phys. Rev. C **68**, 014320 (2003).
[20] T. K. Deague *et al*., Nucl. Phys. **A139**, 501 (1969).
[21] M. Herman, EMPIRE, nuclear reaction model code, available at http://www.nndc.bnl.gov/empire219/
[22] L. Y. Lowie *et al*., Phys. Rev. C **59**, 1119 (1999).
[23] S. F. Mughabghab, *Atlas of Neutron Resonances*, 5th ed. (Elsevier, New York, 2006).
[24] L. M. Bolinger, in *Experimental Neutron Resonance Spectroscopy*, edited by J. A. Harvey (Academic, New York, 1970).
[25] D. De Frenne and E. Jacobs, Nucl. Data Sheets **72**, 1 (1994).
[26] C. L. Duncan and K. S. Krane, Phys. Rev. C **71**, 054322 (2005).
[27] E. S. Macias, M. E. Phelps, D. G. Sarantites, and R. A. Meyer, Phys. Rev. C **14**, 639 (1976).
[28] D. Newton, A. E. R. Tourbeau, A. L. Anderson, and R. A. Meyer, Int. J. Appl. Radiat. Isotop. **29**, 188 (1978).
[29] L. Seren, H. N. Friedlander, and S. H. Turkel, Phys. Rev. **72**, 888 (1947).